# Densification and phase formation in seeded, reactively sintered $Sr_{0.53}Ba_{0.47}Nb_2O_6$ ceramics

C. DURAN*, G. L. MESSING, S. TROLIER-McKINSTRY
*Materials Science and Engineering Department, Materials Research Institute,
The Pennsylvania State University, University Park, PA, 16802, USA*
*E-mail: glm2@psu.edu*

$Sr_{0.53}Ba_{0.47}Nb_2O_6$ (SBN53) ceramics were reactively sintered from $SrNb_2O_6$ and $BaNb_2O_6$ powders. The formation temperature decreased from $1260°C$ for unseeded samples to $1130°C$ for the samples with 15.4 wt% seeds plus 0.85 mol% $V_2O_5$ at a heating rate of $4°C/min$. For the $V_2O_5$-free samples, the activation energy was lowered from $554 \pm 15$ kJ/mol for unseeded samples to $241 \pm 17$ kJ/mol for the samples with 15.4 wt% seeds. In the $V_2O_5$-containing samples, densification and phase formation occurred simultaneously. In the $V_2O_5$-free samples, however, phase formation was completed before densification. In both cases, ceramics with $\geq 95\%$ relative density were obtained. In all cases, SBN53 formed directly, rather than via a variety of intermediate SBN solid solutions. The microstructure evolution was also studied. © *2002 Kluwer Academic Publishers*

## 1. Introduction

Reactive sintering is a process in which chemical reaction and densification are both achieved in the same heat treatment. The two steps can occur in sequence or concurrently, depending on the material and processing variables [1]. For example, smaller particle size or external pressure increases the densification rate compared to the reaction rate [2].

Typically, reactive sintering is done by sintering either the constituent oxides or intermediate products [3, 4], which eliminates the prereaction (or calcination) step(s) and imparts an additional driving force for sintering due to the free energy of the chemical reaction. However, difficulty and complexity in controlling the reaction processes may outweigh these advantages [1]. Yangyun and Brook [2], for example, reported that reactive sintering does not usually yield a chemically homogeneous product with controlled microstructure. They further proposed that products with a high density and controlled microstructure can be obtained if the densification takes place before the chemical reaction. However, Rahaman and De Jonghe [1] found that the fundamental concept in reactive sintering is the degree of microstructural disruption caused by the chemical reaction because, in the case of no microstructural disruption, sintered ceramics with high density and controlled grain size are not dependent on whether the reaction occurs prior to, or after, the densification.

Reactive sintering has been applied to the sintering of $(Sr,Ba)Nb_2O_6$ (SBN) ceramics and was found to be better than conventional sintering in that the latter resulted in low densification and cracking due to abnormal grain growth [4–6]. When SBN is synthesized from

its respective oxides, $SrNb_2O_6$ and $BaNb_2O_6$ were reported to be the final reaction products [7]. Phase formation takes place by forming necks between the particles in the early stage of reactive sintering, and then compositional homogenization (e.g., chemical reaction) takes place as interdiffusion of ions occurs through these necks. It was found that the densification occurs very rapidly following homogenization as a result of the high driving force for the porous, fine-grained, and uniform microstructure [4].

The goal of this study is to determine how seeding and the presence of a liquid phase change the temperature for densification and phase transformation in SBN53 ceramics. $KSr_2Nb_5O_{15}$ (KSN) is a suitable seed material for SBN crystallization during reactive sintering because KSN has the same crystal structure (i.e., tetragonal tungsten bronze (TTB)) as SBN and the lattice parameter difference is less than 0.5% in both $a$ and $c$ directions at room temperature [8, 9]. It has also been shown that SBN60 single crystals can be used as a seed material to grow KSN single crystals by the Czochralski technique [10].

The effect of liquid phase on densification and reaction kinetics is also considered. In the literature, liquid phase sintering of SBN ceramics has been attempted, both intentionally and unintentionally, to promote densification at lower temperatures. Lee and Freer [5, 6] reported that $Nb_2O_5$-excess grain boundaries gave rise to unintentional liquid formation at temperatures $\geq 1260°C$ in the conventional sintering of SBN60 ceramics. Nishiwaki *et al.* [11–13] conventionally sintered SBN30 ceramics in the presence of PbO, $Bi_2O_3$, $Nb_2O_5$, and $V_2O_5$ (0.5 or 1 mol%) and found that only

---

$Nb_2O_5$ and $V_2O_5$ accelerated densification. Therefore, in this work $V_2O_5$ and excess $Nb_2O_5$ were selected as liquid phase formers.

## 2. Experimental procedure

$SrNb_2O_6$ (SN) and $BaNb_2O_6$ (BN) powders were used to prepare $Sr_{0.53}Ba_{0.47}Nb_2O_6$ (SBN53) ceramics by reactive sintering. SN and BN were prepared separately by ball milling $SrCO_3$ (Alfa) or $BaCO_3$ (J.T. Baker) and $Nb_2O_5$ (H.C. Starck, Ceramic grade) for 24 h in ethanol using zirconia balls. The ethanol was evaporated during fast stirring to avoid differential settling. The powder mixtures were dried at 100°C for 24 h, and calcined at 1050°C for 5 h. Using the same procedure, KSN powder was prepared by the solid state reaction of $K_2CO_3$ (J.T. Baker), $SrCO_3$, and $Nb_2O_5$ at 1250°C for 5 h in a closed $Al_2O_3$ crucible. X-ray diffraction (XRD) showed the formation of SN, BN, and KSN after calcination.

Appropriate amounts of SN, BN, and KSN powders were mixed with a vinyl-based (Ferro 73210) binder solution and (Ferro M1111) modifier (Electronic Materials Division, MSI products group) for tape casting. For some compositions, $V_2O_5$ (0.85 mole%) was added as a liquid phase former during sintering. Table I summarizes the sample designation, KSN concentration, and initial amount of additives in the SBN53 samples. Extra BN powder was added to compensate for the strontium and niobium introduced by the KSN seeds. However, the potassium and some of the excess niobium from the KSN could not be compensated for in the final composition. Therefore, the concentrations of $K_2O$ and $Nb_2O_5$ increase with increasing KSN concentration. The slurry was prepared by ball milling the powder mixture, binder solution, and modifier for 24 h in toluene using 1-mm zirconia balls. Each slurry was tape cast on a glass substrate at a casting speed of 7 cm/sec and a blade gap of 200 $\mu$m. After 24 h drying at room temperature, tapes were cut and laminated at 83 MPa. Organics were burned out by heating at 0.5°C/min to 500°C and then holding for 2 h. Scanning electron microscopy (SEM) of the green samples showed that the powders were ~1 $\mu$m in size.

For kinetic analysis, the samples were heated at 4, 7, and 10°C/min to temperatures between 900 and 1450°C, and then air-quenched. Initial and final dimensions in the thickness direction were measured and the amount of shrinkage was calculated. The sample density was determined by the Archimedes technique. The quenched samples were ground for XRD analysis. The scan rate was 1°2$\theta$ per min with a step size of 0.02°. The strongest line intensities of SBN (2$\theta$ = 32.054°) (JCPDS # 39-265), KSN (2$\theta$ = 32.077°) (JCPDS # 34-108), SN (2$\theta$ = 29.211°) (JCPDS # 28-1243), and BN (2$\theta$ = 28.245°) (JCPDS # 32-77) were integrated to find the peak areas, using curve fitting. For BN, the second most intense peak was used because the main BN peak at 2$\theta$ = 29.625° corresponds to the second most intense peaks of SBN and KSN. The fraction of SBN53 formed was calculated by comparing the integrated peak areas of the (SBN and/or KSN) to SN + BN. For the compositions without KSN seeds (e.g., R0 and RV0), only the SBN peaks were used to determine the extent of phase formation. However, for the others, the sum of the SBN and KSN main peaks was used because their 2$\theta$ peak positions are too close to be distinguished.

A nonisothermal reaction kinetics equation [14] was used to find the activation energy. For a constant heating rate, $\beta$:

$$\ln[\beta \cdot (d\alpha/dT)] = \ln[Af(\alpha)] + (-Q/RT) \qquad (1)$$

where $A$ is a frequency factor, $Q$ is the activation energy, $R$ is the gas constant, $T$ is the absolute temperature, and $\alpha$ is the reaction fraction. The function $f(\alpha)$ can be considered to be constant at a fixed value of $\alpha$ if the particle size remains unchanged during the reaction. The activation energy is determined by plotting $\ln[\beta \cdot (d\alpha/dT)]$ vs. $1/T$ at different heating rates for a constant $\alpha$ value.

For sintering experiments, samples were heated at 7°C/min to 1200–1400°C and held at temperature for 1 min to 12 h. For microstructure analysis, samples were polished to 0.3 $\mu$m using fine $Al_2O_3$ powder and then thermally etched 100°C below the sintering temperature for 1 h.

## 3. Results and discussion
### 3.1. Densification and reaction kinetics in the quenched samples
#### 3.1.1. Densification behavior
Fig. 1 shows the densification behavior as a function of quenching temperature and composition, at a heating rate of 7°C/min. The relative density was calculated based on the theoretical density of SBN52 (5.33 g/cc) [15], which is close to the composition of interest. R0 and R15 samples have a steep increase in densification after 1250 and 1200°C, respectively, and reach full density above 1400°C. Densification in the RV0 and RV15 samples, however, starts just after 900°C and increases continuously until 1200–1300°C, depending on the KSN content, and then remains constant. The onset of densification in the RV0 and RV15 samples can be attributed to the melting of $V_2O_5$ at 690°C. The density slightly increases with decreasing heating rate. It was observed that KSN slows densification in the $V_2O_5$-containing samples, and improves it in the $V_2O_5$-free samples. The other samples with various amounts of

TABLE I Sample designation, KSN content, and additive contribution in SBN53

| Sample designation[a] | $V_2O_5$ (wt%) | KSN content (wt%) | Additive contribution (wt%) | |
|---|---|---|---|---|
| | | | $K_2O$ | $Nb_2O_5$ |
| R0 | 0 | 0 | 0 | 0 |
| RV0 | 0.37 | | | |
| R5 | 0 | 5 | 0.26 | 0.72 |
| RV5 | 0.37 | | | |
| R9 | 0 | 9.1 | 0.47 | 1.32 |
| RV9 | 0.37 | | | |
| R15 | 0 | 15.4 | 0.80 | 2.23 |
| RV15 | 0.37 | | | |

[a]R and RV denote $V_2O_5$-free and $V_2O_5$-containing samples, respectively.
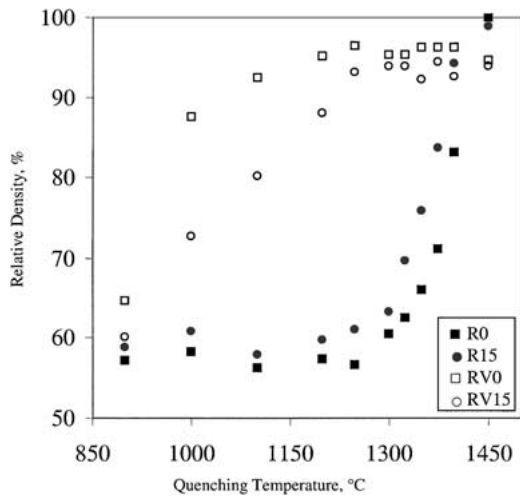
**Figure 1** Densification graphs as a function of composition. Heating rate is 7°C/min.

KSN show trends in between the end member compositions. These data will be discussed later together with the sintered samples.

All samples shrank ~17% through the thickness upon full densification. In addition, densification curves indicate that there was no volumetric expansion during reactive sintering.

### 3.1.2. Phase formation

Fig. 2 shows the XRD patterns for the RV0 samples at various stages of reaction when heated at $\beta = 4$°C/min. The XRD pattern of the sample after burnout (500°C) is given as a reference for the $\alpha = 0$ case. The amount of SBN53 increases with the reaction temperature. At 900°C, an unknown phase starts to appear and, at the same time, BN peaks disappear. The amount of this unknown phase first increases up to 1000°C and then gradually disappears at higher temperature. The other char-
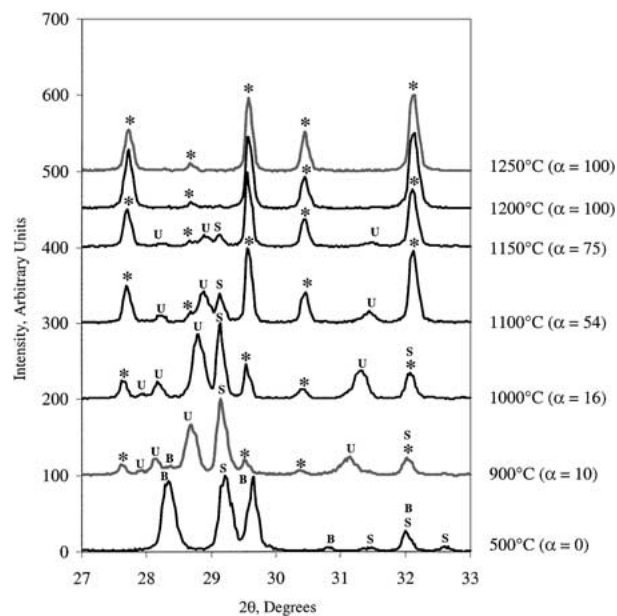


**Figure 2** Phase evolution in the RV0 samples as a function of quenching temperature. Heating rate is 4°C/min. *: SBN53, S: SN, B: BN, U: Unknown. $\alpha$ is given in %.
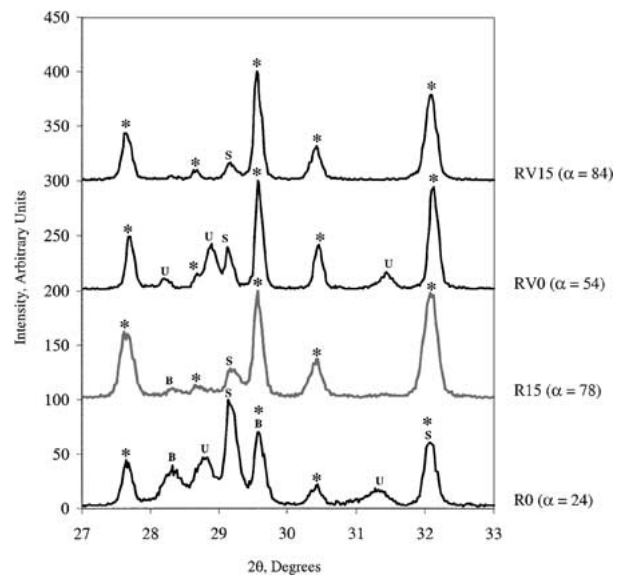


**Figure 3** Phase evolution in the samples quenched from 1100°C. Heating rate is 4°C/min. *: SBN53, S: SN, B: BN, U: Unknown.

acteristic is that peak positions of the unknown phase steadily shift to higher diffraction angles with temperature. Note that the integrated peak area of the most intense unknown phase was also taken into account in the calculation of $\alpha$.

Fig. 3 shows that a higher seed content, assisted by a liquid, increases $\alpha$ considerably (e.g., R0 vs. RV15) at the same temperature. It is apparent that the unknown phase also forms in the R0 samples but the BN peaks do not disappear. In both cases, the amount of the unknown phase decreases with increasing seed content and temperature, and its formation is almost independent of the heating rate. No known phases in the SrO-BaO-Nb$_2$O$_5$-V$_2$O$_5$ system were found to match the unknown phase.

The existence of the unknown phase has not been reported in the literature. Fang *et al*. [7] proposed that BN and SN are the last intermediate products in SBN50 formation from the respective oxides and that they form at 800–1100°C. The SBN50 forms by gradual consumption of SN and BN between 1000–1150°C. Nishiwaki *et al*. [11] reported that SrNb$_2$V$_2$O$_{11}$ and BaNb$_2$V$_2$O$_{11}$ form at 700 to 800°C and melt at around 900°C when V$_2$O$_5$ (1 mol%) is present. In this study, however, the unknown phase forms even in the V$_2$O$_5$-free compositions, although the amount is small compared to the V$_2$O$_5$-containing samples. This indicates that the presence of a liquid favors the formation of this phase. More study is required to identify this unknown phase. Table II shows the variation in the diffraction angle of

**TABLE II** Change in the diffraction angle ($2\theta$) of the main peak (311) of the SBN

| $\alpha^a$ | R0 (°) | RV0 (°) | R15 (°) | RV15 (°) |
|---|---|---|---|---|
| 20–30 | 32.06 | 32.08 | 32.14 | 32.08 |
| 70–80 | 32.10 | 32.10 | 32.08 | 32.10 |
| 100 | 32.14 | 32.14 | 32.12 | 32.10 |
| $\Delta 2\theta^b$ (°) | 0.08 | 0.06 | 0.02 | 0.02 |

[a]At $\beta = 4$°C/min.
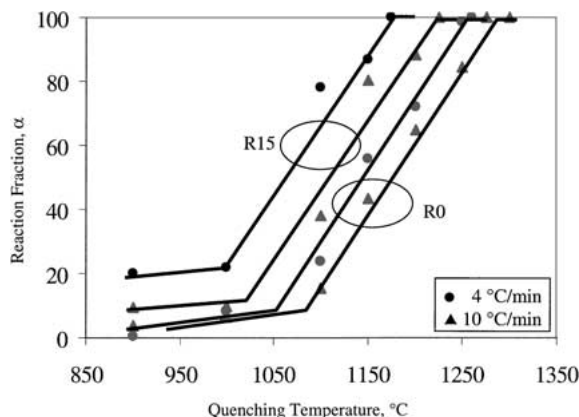[b]Between $\alpha$ values of 20–30 and 100.

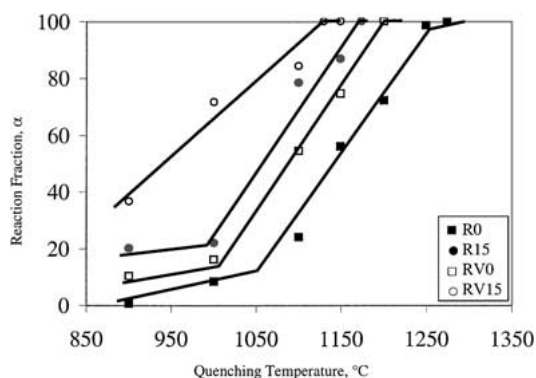*Figure 4* SBN53 formation ($\alpha$) as a function of KSN seed content and heating rate.



*Figure 5* SBN formation as a function of KSN seed content at a heating rate of 4°C.

the main peak (311) of SBN as a function of $\alpha$ and composition at $\beta = 4°C/min$. The change in the diffraction angle ($\Delta 2\theta$) between $\alpha = 20$–30 and 100 is very small, which indicates that the desired SBN composition forms directly, rather than via a variety of intermediate SBN solid solutions (i.e., other than SBN53). A similar result was also observed by Lee and Fang [4]. They also suggested that diffusion of strontium and barium ions through the SBN phase during the reaction can cause a slight shift in the main peak position.

Fig. 4 shows the reaction fraction ($\alpha$) of SBN53 as a function of heating rate and seed content. The lines are drawn to guide the eye. The curves show a sigmoidal shape. For each composition, $\alpha$ decreases with increasing heating rate at the same temperature. In addition, increasing the seed content sharply accelerates phase formation. For example, the R15 samples reach $\alpha = 100$ at 1175°C ($\beta = 4°C/min$) compared to 1260°C ($\beta = 4°C/min$) and 1275°C ($\beta = 10°C/min$) in the R0 samples. Also, the temperature at which detectable reaction ($\alpha \cong 20$) occurs decreases with increasing seed content. Fig. 5 indicates that introduction of a liquid during the reaction drastically improves $\alpha$ at lower temperatures ($\beta = 4°C/min$). Again the lines are drawn to guide the eye. For instance, the phase formation is complete at 1260°C for the R0 samples and 1130°C for the RV15 samples. These results indicate that the phase formation is accelerated because the liquid phase provides a path for faster transport and that the KSN seed parti-

cles lower the activation energy for the SBN formation by epitaxy.

Comparison of the densification (Fig. 1) and phase formation (Fig. 5) behaviors reveals that the presence of a liquid during the reaction sintering changes the sequence of whether densification or the phase formation takes place first. For example, densification starts after 1250°C and phase formation ($\alpha = 100$) is complete at 1275°C for the R0 samples ($\beta = 7°C/min$), which shows that phase formation is initiated prior to the densification. However, the densification and phase formation take place simultaneously in the RV0 samples because when the phase formation is finished at 1225°C ($\beta = 7°C/min$), the samples have already reached $\geq 95\%$ relative density. In both cases, ceramics with $\geq 95\%$ relative density were obtained, which indicates that it is not very critical whether densification occurs prior to, simultaneously, or after the phase formation during the reactive sintering of SBN ceramics.

### 3.1.3. Reaction kinetics

The activation energy was calculated using Equation 1 for the R0–R15 samples. The particle size increases only slightly ($\sim \leq 2$–3 $\mu m$) with temperature during SBN53 formation. Thus, the $f(\alpha)$ term can be considered constant at a fixed value of $\alpha$ [14]. For the RV0-RV15 samples, however, particle (or grain) size changes considerably with temperature due to the melting of $V_2O_5$ at 690°C, and hence the $f(\alpha)$ term may not be constant.

Fig. 6 shows a plot of ln $[\beta \cdot (d\alpha/dT)]$ vs. $1/T$ at $\beta = 4$, 7, and 10°C/min for the R0 samples at $\alpha$ of 30, 50, and 70. The lines are results of linear curve fitting to the experimental data at a constant $\alpha$. The ($d\alpha/dT$) values were calculated from the slopes of the $\alpha$ vs. $T$ plots (i.e., curve fitting to the linear section in Fig. 5). For each composition, the lines are parallel to each other at constant $\alpha$, which shows that one mechanism dominates during the entire reaction. Lee and Fang [14] also observed parallel lines for the formation of SBN50 to SBN70. Fig. 7 indicates that the slope decreases with increasing KSN seed content. The activation energy calculated from the slopes of the $\ln[\beta \cdot (d\alpha/dT)]$ vs. $1/T$ plots is $554 \pm 15$ kJ/mol for the R0, $239 \pm 36$ kJ/mol for
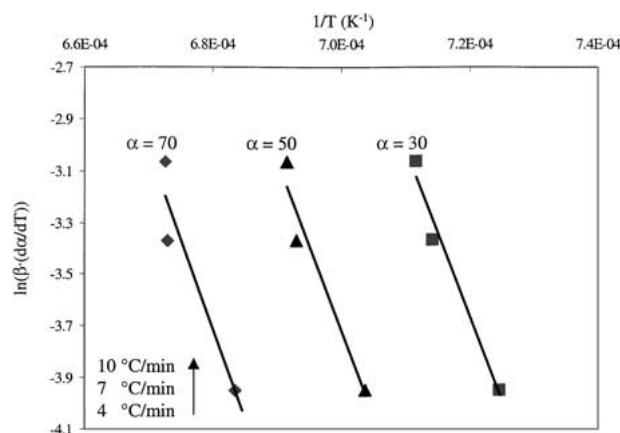


*Figure 6* Plot of $\ln(\beta \cdot (d\alpha/dT))$ vs. $1/T$ for the R0 samples as a function of $\alpha$ and $\beta$.
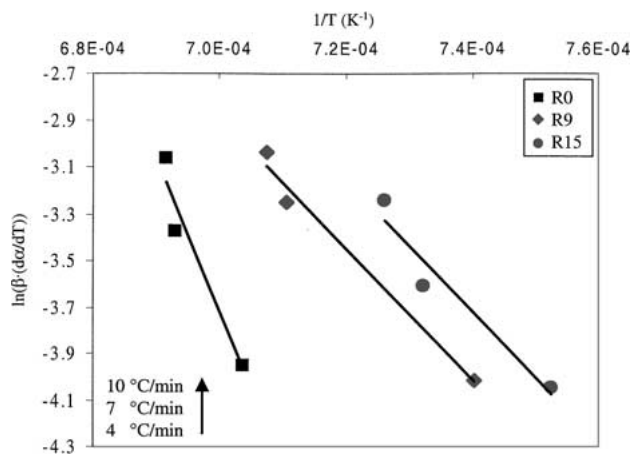
*Figure 7* Plot of $\ln(\beta \cdot (d\alpha/dT))$ vs. $1/T$ as a function of heating rate at a constant $\alpha = 50$.



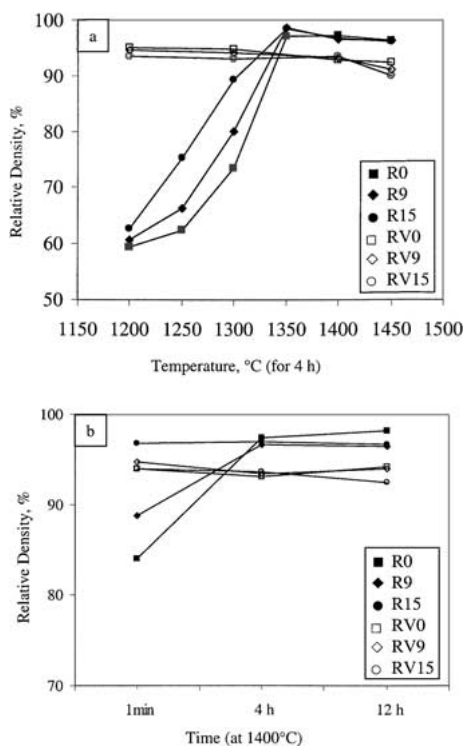*Figure 8* Densification graphs of the sintered samples as a function of (a) sintering temperature and (b) time. $\beta = 7°C/min$.

the R9, and $241 \pm 17$ kJ/mol for the R15 samples. This result shows that introduction of isostructural KSN seed particles drastically decreases the energy barrier for SBN53 formation. An activation energy of 735 kJ/mol was reported for SBN50 formation in the literature [14]. The lower activation energy (i.e., $554 \pm 15$ kJ/mol for R0) obtained in this study may be attributed to the difference in the processing variables such as green body formation (tape casting vs. dry pressing), initial particle size and mixing of the reactants.

It is expected that the $V_2O_5$-containing samples (RV0 to RV15) would have a lower activation energy because the liquid enables faster transport for SBN formation during the reaction. This conclusion is supported by the fact that the RV0 and RV15 samples are completely reacted at lower temperatures than R0 or RV0, as seen in Fig. 5.

## 3.2. Densification and microstructure evolution in the sintered samples
### 3.2.1. Densification
Fig. 8 shows the densification behavior as a function of sintering conditions and composition. The RV0–RV15 samples have almost constant density of 93–95% between 1200 to 1450°C after sintering for 4 h due to the liquid phase sintering, which is consistent with Fig. 1. The sintered R0–R15 samples reach densities of 97–99% at 1350°C (Fig. 8a) compared to 1400–1450°C for the quenched samples (Fig. 1), due to the longer hold times. Note that they have ~60% relative density at 1200°C. The densities of the sintered samples remain almost constant ($\geq$93%) with sintering time at 1400°C except for samples R0 and R9 (Fig. 8b). These samples require longer time to reach higher densities.

Comparison of Figs 1 and 8a indicates that the densification decreases with increasing KSN content in the RV0–RV15 samples (Fig. 1) and vice versa in the R0–R15 samples (Fig. 8a). This difference in the densification behaviors stems mainly from the presence of a liquid phase and homogenization of ions in the tungsten bronze structure.

A liquid phase is present all the time for the RV0–RV15 samples due to the melting of $V_2O_5$. For the R0-R15 samples, however, a liquid forms due to excess $Nb_2O_5$ introduced from the KSN seeds. Therefore, with increasing KSN content, the liquid amount increases and its formation temperature decreases. The liquid formation due to excess $Nb_2O_5$ was observed in conventional sintering of SBN60 ceramics [5, 6]. For the KSN-free samples (i.e., R0 and RV0), SN and BN react to form SBN in a single homogenization step. For the KSN-containing samples, however, the first homogenization step is again the formation of SBN in which, depending on the seed content, SBN either nucleates on the seed particles and/or forms between SN and BN. The second reaction is the formation of the solid solution between SBN and KSN, during which excess $Nb_2O_5$ forms a liquid in the R0–R15 samples.

The homogenization process is closely related to the crystal structure. There are six interstitial (A) sites in the TTB structure, five of which are occupied by Sr/Ba ions. Because the $A_1$ site (15-fold coordination) is larger than the $A_2$ site (12-fold coordination), larger $Ba^{2+}$ ions predominantly prefer to occupy the $A_1$ sites and smaller $Sr^{2+}$ ions occupy either the $A_2$ site or a combination of $A_2$ and $A_1$ sites [15]. Also, the $K^+$ ions go to vacant A sites and fill the structure [16, 17]. As the KSN content changes, the distribution of these ions and remaining vacant sites may change in the A sites. For example, the lattice will be distorted more as the fraction of $Sr^{2+}$ ions increases on the $A_1$ site because the size of this site is relatively larger than the $Sr^{2+}$ ion. Fang *et al.* [7] reported that a high concentration of $Sr^{2+}$ ions in the $A_1$ site inhibits the formation of SBN at low calcination temperatures due to increased lattice distortion. In addition, introduction of $K^+$ ions into the A sites might also promote lattice distortion. The more-distorted lattice would make the diffusion of ions through the product layer more difficult. This might account for slower densification in the RV0–RV15 samples with
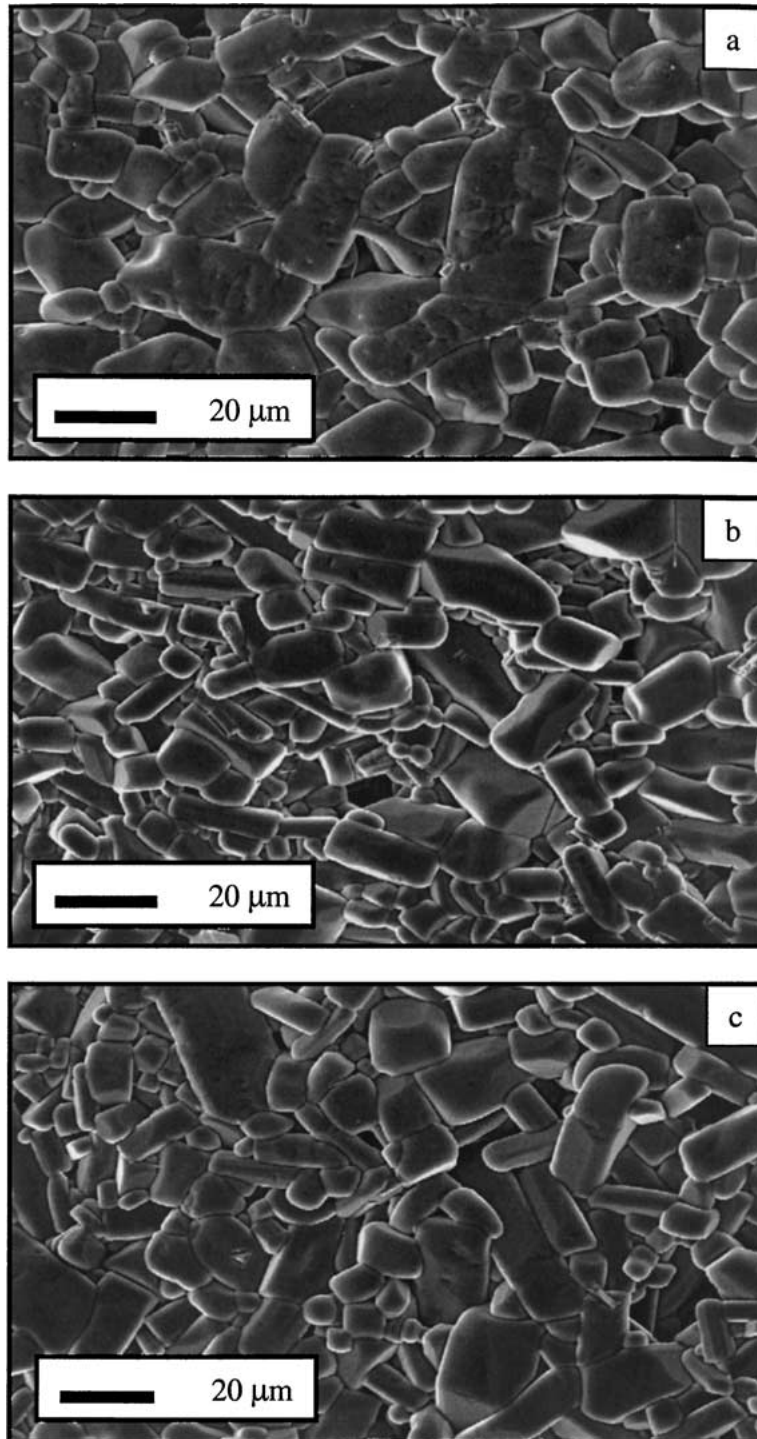
*Figure 9* Microstructure development in the $V_2O_5$-containing samples sintered at 1400°C for 4 h; (a) RV0, (b) RV5, and (c) RV15.

increasing KSN content (Fig. 1). The homogenization of SN and BN to form SBN53 in the RV0 samples is faster compared to the additional $K^+$ homogenization with increasing KSN content. Particle rearrangement due to liquid formation can also promote densification at lower temperatures compared to the R0-R15 samples (see Fig. 1).

Because the R0–R15 samples do not have a liquid at lower temperatures, the compositional homogenization to form SBN53 and the subsequent solid solution with KSN takes place in the solid state after 1200°C. Therefore, a sharp chemical gradient difference between different regions promotes the diffusion of the ions in the absence of a liquid. Lee and Fang [4] stated that

the densification rate of reaction-sintered SBN50 and SBN60 samples could be pronouncedly enhanced when the homogenization is almost completed. The reason is that homogenization due to a chemical gradient does not change the state of the microstructure because it happens through the necks. A uniform, highly porous, and fine grain microstructure is retained during the homogenization steps, as will be seen in the next section. Interdiffusion is a dominant process when the necks form because the material transport due to the chemical gradient is more important than the material flow due to the surface curvature [18]. When the necks grow larger, the interdiffusion of ions becomes easier and predominant, which stops additional sintering until the

homogenization is further advanced [4, 19]. After the disappearance of the chemical gradient, the retained high surface area microstructure induces a high driving force for further densification, which can sharply increase densification. Because the temperature at which SBN53 formation is complete decreases with increasing KSN seed content (e.g., 1210°C for the R15 and 1275°C for the R0 samples ($\beta = 7$°C/min)), the density increases sharply after 1200°C for the R15 samples.

Therefore, the amount of liquid phase, the temperature at which it forms, and the possibility of $K^+$ con-

tribution to the lattice distortion are all competing processes. Each is dependent on the presence and amount of the KSN phase, which markedly affects the densification behavior of the SBN ceramics. It is evident from Figs 1 and 8 that the presence of a liquid is the primary contributor to attain a high density at lower temperatures.

### 3.2.2. Microstructure evolution

Fig. 9 shows the microstructure development in the $V_2O_5$-containing samples sintered at 1400°C for 4 h.
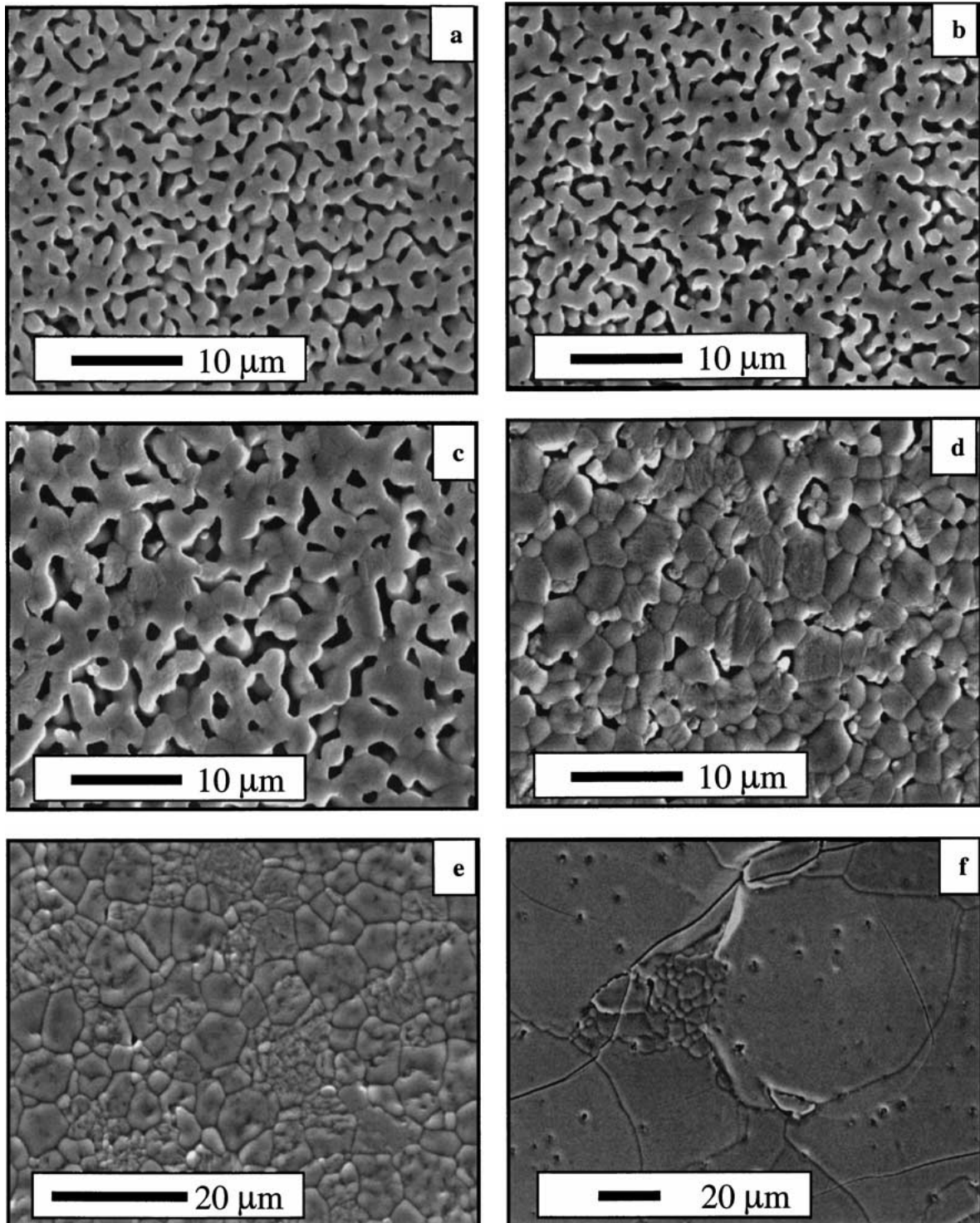


*Figure 10* Microstructure evolution in the R0 (left column) and R15 (right column) samples as a function of sintering temperature; (a and b) 1200°C, (c and d) 1300°C, and (e and f) 1400°C for 4 h.
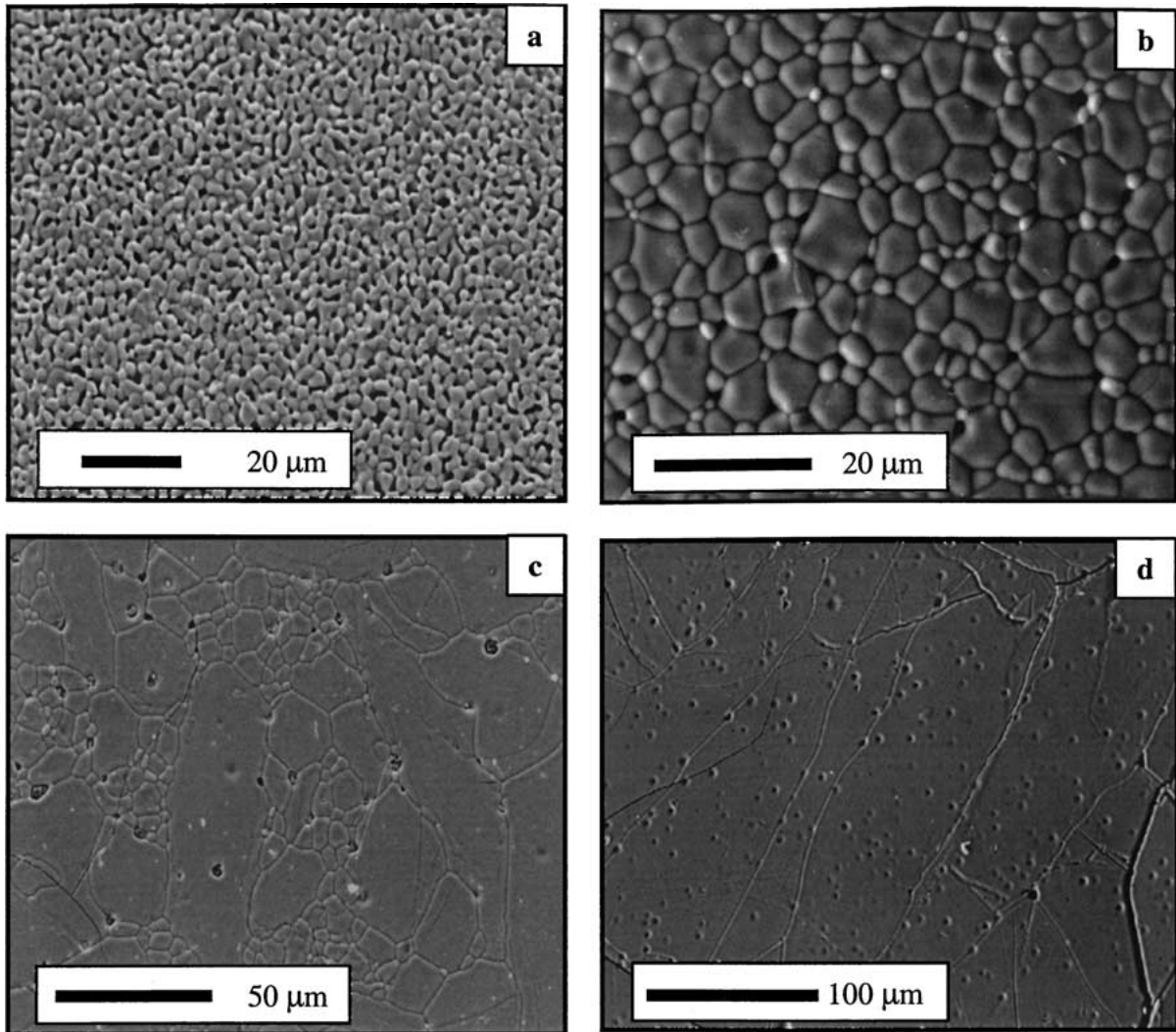
*Figure 11* Microstructure evolution in the R0 (left column) and R15 (right column) samples as a function of sintering time; (a and b) 1 min, (c and d) 12 h at 1400°C.

The samples have elongated grains of various aspect ratios due to liquid phase sintering. They have the same characteristic microstructures irrespective of sintering temperature and time. Figs 10 and 11 show the microstructure evolution for the R0 and R15 samples as a function of sintering temperature and time, respectively. At 1200°C, samples are very porous and have a fine grain size of ~2 $\mu$m. With increasing temperature, neck growth continues and the sintering rate rises. At 1300°C, the pore structure is closed and is mostly concentrated at the triple points in the R15 sample, while RO has open porosity. At 1400°C, the R0 sample is completely dense. In contrast, the R15 sample has undergone exaggerated grain growth and cracks on cooling as a result. Fig. 11a and b shows that the R15 sample has a very dense microstructure after sintering 1 min at 1400°C compared to the very fine and porous microstructure for the R0 sample. The microstructures of the R15 sample at higher temperatures and longer times (Figs 10f and 11d) show a duplex microstructure consisting of mm-sized grains together with smaller grains. Cracking and spherical porosity entrapped within the big grains are easily observable.

Despite the homogenization step, the R0 samples show abnormal grain growth behavior (Fig. 11c). This suggests that, even in a stoichiometric mixture of SN + BN, abnormal grain growth can be observed, though at high sintering temperatures and times (e.g., $T >$ 1400°C for 12 h). Abnormal grain growth in the R15 sample, for example, started earlier (e.g., after sintering at 1400°C for 4 h) due to the higher liquid phase content (e.g., more excess $Nb_2O_5$). The duplex microstructure formation in these samples can be attributed to the non-uniform wetting of the grains by the liquid. That is, grain growth localizes before the liquid spreads out, which causes liquid phase sintering in selected parts of the specimen. As seen for the R15 sample in Fig. 11b, a bimodal grain size distribution is observed after sintering for 1 min at 1400°C. The presence of a liquid film increases the grain boundary mobility by providing a path for rapid diffusion, especially for the wetted grains. This gives rise to the formation of very big grains ($>$ 100 $\mu$m) and entrapped porosity within these grains. Similar microstructure evolution was also reported in conventional sintering of SBN60 ceramics [5, 6].

Microstructural evolution indicates that samples with high density and uniform grain size are obtained at different KSN contents. Abnormal grain growth in the R0-R15 samples takes place, only when the samples are overheated.

## 4. Conclusions

$Sr_{0.53}Ba_{0.47}Nb_2O_6$ (SBN53) ceramics were reactively sintered from $SrNb_2O_6$ and $BaNb_2O_6$ powders. $KSr_2Nb_5O_{15}$ (KSN) was used as a seed material to accelerate the SBN53 formation. An unknown phase started to form in the samples during the SBN53 formation. The amount of this phase was greater in the $V_2O_5$-containing samples, and decreased with increasing seed content and reaction temperature. $V_2O_5$-containing samples densified at lower temperatures due to the $V_2O_5$ liquid phase and they reached maximum density at $T \leq 1250°C$, compared to $T \geq 1350°C$ in the $V_2O_5$-free samples. The heating rate did not affect the densification much, except that the density was slightly higher at lower heating rates.

The presence of a liquid changed the sequence of the reactive sintering. In the $V_2O_5$-containing samples, densification and phase formation occurred simultaneously. In the $V_2O_5$-free samples, however, the phase formation was completed before densification. In both cases, ceramics with $\geq 95\%$ relative density were obtained, indicating that it is not critical whether the densification or phase formation takes place first.

The formation temperature for SBN53 was lowered substantially by adding seeds, decreasing the heating rate, and/or introducing a liquid. For example, the temperature decreased from $1260°C$ for the samples with no seeds to $1130°C$ for the samples with 15.4 wt% seeds plus 0.85 mol% $V_2O_5$ at a heating rate of $4°C$/min. For the $V_2O_5$-free samples, the activation energy was lowered from $554 \pm 15$ kJ/mol for the samples with no seeds to $241 \pm 17$ kJ/mol for the samples with 15.4 wt% seeds. In addition, for all compositions, the SBN53 was formed directly, rather than via a variety of intermediate SBN solid solutions (i.e., other than SBN53).

Samples with high density and uniform grain size were obtained at different KSN contents. Unlike the $V_2O_5$-containing samples, abnormal grain growth in the $V_2O_5$-free compositions took place, only when the samples were oversintered.

## References

1. M. N. RAHAMAN and L. C. DE JONGHE, *J. Amer. Ceram. Soc.* **76** (1993) 1739.
2. S. YANGYUN and R. J. BROOK, *Sci. Sintering* **17** (1985) 35.
3. W.-S. HONG, L. C. DE JONGHE, X. YANG and M. N. RAHAMAN, *J. Amer. Ceram. Soc.* **78** (1995) 3217.
4. W.-J. LEE and T.-T. FANG, *ibid.* **81** (1998) 1019.
5. H.-Y. LEE and R. FREER, *J. Appl. Phys.* **81** (1997) 376.
6. *Idem.*, *J. Mater. Sci.* **33** (1998) 1703.
7. T.-T. FANG, N.-T. WU and F.-S. SHIAU, *J. Mater. Sci. Lett.* **13** (1994) 1746.
8. R. R. NEURGAONKAR, W. K. CORY and J. R. OLIVER, *Ferroelectrics* **51** (1983) 3.
9. R. R. NEURGAONKAR, J. R. OLIVER and L. E. CROSS, *ibid.* **56** (1984) 31.
10. R. R. NEURGAONKAR, W. W. HO, W. K. CORY, W. F. HALL and L. E. CROSS, *ibid.* **51** (1984) 185.
11. S. NISHIWAKI, J. TAKAHASHI and K. KODAIRA, *J. Ceram. Soc. Japan*, *Int. Edition* **103** (1995) 1233.
12. *Idem.*, *Jpn. J. Appl. Phys.* **33** (1994) 5477.
13. *Idem.*, *J. Ceram. Soc. Japan*, Int. Edition **104** (1996) 413.
14. W.-J. LEE and T.-T. FANG, *J. Amer. Ceram. Soc.* **81** (1998) 193.
15. R. R. NEURGAONKAR, W. K. CORY, J. R. OLIVER, E. J. SHARP, G. L. WOOD and G. J. SALAMO, *Ferroelectrics* **142** (1993) 167.
16. K. C. MOULI, K. H. RAO, P. S. V. SUBBA RAO and A. BHANUMATHI, *ibid.* **67** (1986) 169.
17. T. KIMURA, S. SAIUBOL and K. NAGATA, *J. Ceram. Soc. Japan*, Int. Edition **103** (1995) 132.
18. P. F. STABLEIN JR. and G. C. KUCZYNSKI, *Acta Metall.* **11** (1963) 1327.
19. G. C. KUCZYNSKI, in "Sintering and Related Phenomena," edited by G. C. Kuczynski, N. A. Hooton and C. F. Gibbon (Gordon and Breach, NY, 1967) p. 685.